Magnon Energy of Nickel*

E. D. THOMPSON AND J. J. MYERS†
Case Institute of Technology, Cleveland, Ohio
(Received 28 July 1966)

The spin-wave energy in nickel is calculated along the principal axis directions from the center to the surface of the Brillouin zone, the calculation being based upon the theoretical energy bands of nickel as given by Hanus. The splitting of the up- and down-spin d bands is treated as a parameter, adjusted to give the experimentally observed long-wavelength spin-wave energy. The temperature dependence of the magnetization is calculated on the basis of the spin-wave energies. It is found that the temperature analogous to the Debye temperature of lattice vibrations is of the order of 10^3 °K, rather than 10^4 °K, as simple models yield, that the number of Fourier coefficients (in real space) required to fit the dispersion curve corresponds to the six nearest atomic planes, that the energy gap for single-particle excitations is of the order of 1000°K (although sensitive to the parameters assumed), and that no cutoff momentum is indicated for the strong ferromagnetic assumptions made here. Furthermore, the coefficient of the q^4 term in the dispersion curve and the corresponding coefficient of $T^{5/2}$ in the magnetization law is about a factor of 5–10 larger than that of a nearest-neighbor Heisenberg ferromagnet. The range of validity of $T^{3/2}$ and $T^{5/2}$ terms in the magnetization-temperature law is restricted to temperatures less than 80°K.

I. INTRODUCTION

THE dispersion relation for collective magnetic excitations–spin waves–in the ferromagnetic metals depends in a complicated manner upon the one-electron energies of the magnetic carriers, the splitting between the majority and minority spin bands, and the direct, positive exchange interaction between fluctuating spins on neighboring atomic sites.[1,2] This dispersion relation is obtained as the solution of an integral equation for the case in which the magnetic carriers are contained in a single energy band, or as the solution of a set of coupled integral equations for multiple bands. These equations have been solved analytically for different approximate models,[3] but none of these models approximates even closely the electronic structure of the ferromagnetic transition metals.[4–6] It is our purpose here to present a numerical calculation of the dispersion relation for nickel, based upon its energy band structure as calculated by Hanus.[7]

Two important questions provoked this study: First, is it possible to "explain" the spin-wave mass at long wavelengths in terms of the energy band structure alone without invoking interatomic exchange? Second, is the large spin-wave mass variation with momentum[8,9] explicable without requiring long-range interatomic exchange? The answer found here to both of these questions is yes, but this answer does not negate interatomic exchange, either short- or long-range, from a possible contributing role to the spin-wave spectrum.

Section II of this paper outlines the calculational details and includes the density-of-states function as a side result. Since the integral equation requires the one-electron energies as a function of k vector, Hanus's calculated nickel bands[7] are interpolated using the Slater-Koster scheme,[10] details of which are presented in Appendix A, and the interpolated and calculated bands are compared in this part.

Section III presents the numerical results as a function of disposable parameters still contained in the calculation, namely, the chemical potential, the band splitting, and the interatomic exchange. The dispersion curve is given along the three principal axis directions from the center to the edge of the Brillouin zone, and analytical fitting using both power and Fourier series is carried out. The effects of multiple carrier bands is discussed.

Section IV calculates the temperature-dependent magnetization expected from the calculated spin-wave dispersion, neglecting other contributing thermal excitations. Section V discusses the implications of the calculations and summarizes the results.

II. THE CALCULATION

A. Integral Equation and Defining Parameters

For a ferromagnetic crystalline metal with magnetic carriers contained in a single energy band, the energy of a single-reversed spin state $E(\mathbf{q})$ of pseudomomentum

* This research supported by a National Science Foundation initiation grant.

† Present address: Pennsylvania State University, State College, Pennsylvania.

[1] D. Mattis, *Theory of Magnetism* (Harper & Row, New York, 1965), Chap. 7.

[2] E. D. Thompson, Advan. Phys. 14, 213 (1965).

[3] The most generally used model is that of intra-atomic exchange and a quadratic momentum dependence of the one-electron energies. Inclusion of interatomic direct exchange and a quartic momentum dependence in the model has been done for long-wavelength solutions. Some study has been done on the simple cubic structures with intra-atomic exchange and a one-electron energy dependence, $\epsilon(\mathbf{k}) = -W[\cos(k_x a)+\cos(k_y a)+\cos(k_z a)]$.

[4] L. F. Mattheiss, Phys. Rev. 134, A970 (1964).

[5] J. C. Phillips, Phys. Rev. 133, A1020 (1964).

[6] H. Ehrenreich, H. R. Phillipp, and D. J. Olechna, Phys. Rev. 131, 2469 (1963).

[7] J. G. Hanus, MIT Solid State and Molecular Theory Group Quarterly Progress Report, p. 29, April 1962 (unpublished).

[8] B. E. Argyle, S. H. Charap, and E. W. Pugh, Phys. Rev. 132, 2051 (1963).

[9] R. Weber and P. E. Tannenwald, Phys. Rev. 140, A498 (1965).

[10] J. C. Slater and G. F. Koster, Phys. Rev. 94, 1498 (1954).

$\mathbf{q}$ is given as the solution of the integral equation[2]

$$[\Delta E_d+J(\mathbf{q})-J(\mathbf{0})]N^{-1}$$
$$\times\sum_{\mathbf{k}}[\Delta E_d+\epsilon(\mathbf{k}+\mathbf{q})-\epsilon(\mathbf{k})-E(\mathbf{q})]^{-1}=1. \quad (1)$$

In this equation, ΔE_d is the splitting between up- and down-spin bands, N is the net number of magnetic carriers, $\epsilon(\mathbf{k})$ is the one-electron energy (nonmagnetic) eigenvalue of the Bloch wave $\phi_{\mathbf{k}}(\mathbf{r})$ with wave vector $\mathbf{k}$, and $J(\mathbf{q})$ is the Fourier transform of the interatomic exchange,

$$J(\mathbf{q})=\sum_{\mathbf{R}}{}' \exp(i\mathbf{q}\cdot\mathbf{R})\mathcal{J}(\mathbf{R}),$$

where

$$\mathcal{J}(\mathbf{R})=\int\int d\mathbf{r}d\mathbf{r}'W^*(\mathbf{r})W^*(\mathbf{r}'-\mathbf{R})U(\mathbf{r},\mathbf{r}')$$
$$\times W(\mathbf{r}')W(\mathbf{r}-\mathbf{R}),$$

with

$$W(\mathbf{r}-\mathbf{R})=N_a^{-1/2}\sum_{\mathbf{k}} e^{i\mathbf{k}\cdot\mathbf{R}}\phi_{\mathbf{k}}(\mathbf{r}),$$

the Wannier transform of the Bloch wave, and U the interaction potential between electrons. The sum in Eq. (1) is restricted to those $\mathbf{k}$ vectors in which the majority spin state of vector $\mathbf{k}$ is occupied and the minority spin state of vector $\mathbf{k}+\mathbf{q}$ is unoccupied; i.e., $\epsilon(\mathbf{k})\leq\mu$ and $\epsilon(\mathbf{k}+\mathbf{q})>\mu-\Delta E_d$, where μ is the chemical potential.

The parameters ΔE_d and $J(\mathbf{q})$ [or $\mathcal{J}(\mathbf{R})$] appearing in Eq. (1) are largely unknown,[11] while the one-electron energies $\epsilon(\mathbf{k})$ have been calculated by Hanus[7] and the spin-wave energy $E(\mathbf{q})$ is known for $qa\ll 1$, where a is the length of the cube edge.[12] Accordingly, Eq. (1) is solved as outlined in the following, treating ΔE_d and $J(\mathbf{q})$ as parameters.

A cubical mesh is established in the Brillouin zone, the distance[13] between Γ and X being divided into 16 equal segments, corresponding to 505 distinct stars of the k vectors and 16 384 mesh points in the Brillouin zone. $\epsilon(\mathbf{k})$ is found on these mesh points by interpolating on the nickel bands as calculated by Hanus[7] using the Slater-Koster[10] interpolation formula, a procedure described in Sec. II B and in Appendix A. Two chemical potentials are chosen such that the number of holes per atom of one spin in the d band is 0.6 and 0.44, corresponding respectively to the d band containing all the magnetic carriers and containing 75% of the carriers, the remaining spin density being accounted for by an s-p band spin imbalance[5] in the latter case.

Equation (1) is then solved for sufficiently small $\mathbf{q}$ such that the approximation

$$E(\mathbf{q})=(\hbar^2/2m_{\mathrm{sw}})|q|^2 \quad (2)$$

is found to be valid. In view of the original questions as given in the Introduction, $\mathcal{J}(\mathbf{R})$ is assumed to be zero for all $\mathbf{R}$ and $(1/m_{\mathrm{sw}})$ is found as a function of the band-splitting parameter ΔE_d. Finding ΔE_d such that the spin-wave mass equals the experimental value[12] $m_{\mathrm{sw}}=9.8m_0$ with m_0 the free-electron mass, Eq. (1) is solved for all $\mathbf{q}$ on the mesh in the [100], [110], and [111] directions. Having outlined in general the calculation, we can now proceed to the interpolation on the energy bands and the resultant density of states.

B. Energy-Band Interpolation

Hanus's nickel energy bands[7] were calculated by the augmented-plane-wave (APW) technique with the $\mathbf{k}$ vector restricted to selected symmetry points and directions in the Brillouin zone. Such a calculational technique admixes, in general, wave functions of s, p, d, f, $\cdots$, symmetry about an atomic site, and the concept of s, p, d, $\cdots$, energy bands loses meaning in a strict sense. But more importantly, the magnetic carriers (considered here as holes) are no longer contained in a single energy band and there is no unique way of labeling the bands. Equation (1) is explicit in requiring carriers in one band only, and the extension of (1) to multiple bands[1,2] requires common interaction properties among carriers in a given band. This latter property cannot be met because of the crossing of bands in certain symmetry directions and noncrossing in off-symmetry axes.

For nickel, the major difficulty lies in the crossing and admixing among the $3d$-like, $4s$-like, and $4p$-like bands. In principle,[14] an approximate multiple-band calculation based on the extension to Eq. (1) can be done, but the added complexity and added number of unknown parameters make such a calculation appear unwarranted at the present time. Accordingly, we proceed with a simpler band model than Hanus's, a model calculated by Fletcher[15] and used for chromium[16] and nickel,[5] namely, a model of $3d$ bands overlapped by, but not interacting with, $4s$-$4p$–like bands.

Such noninteracting bands can be obtained by applying the Slater-Koster interpolation procedure[10] to Hanus's bands and by setting those Hamiltonian interpolation parameters equal to zero which represent interaction between these different bands. The details of the interpolation procedure and the resultant parameters are given in Appendix A.

The resultant $3d$ bands, along with those calculated

[11] A summary of the various estimates for ΔE_d has been presented by E. P. Wohlfarth, in *Proceedings of the International Conference on Magnetism, Nottingham, 1964* (Institute of Physics and the Physical Society, London, 1965). Unfortunately, there is no direct experimental observation of this quantity to date. A. J. Freeman, R. K. Nesbet, and R. E. Watson, Phys. Rev. **125**, 1978 (1962) have calculated the nearest-neighbor exchange integral $\mathcal{J}(\mathbf{R})$ for a cobalt diatomic molecule, but relating these calculational results to real metals is most uncertain.

[12] H. Nosé, J. Phys. Soc. Japan **16**, 2475 (1961).

[13] The notation is that of L. P. Bouckaert, R. Smoluchowski, and E. Wigner, Phys. Rev. **50**, 58 (1936).

[14] D. C. Mattis, Phys. Rev. **132**, 2521 (1963).

[15] G. C. Fletcher, Proc. Phys. Soc. (London) **A65**, 192 (1952).

[16] W. M. Lomer, Proc. Phys. Soc. (London) **80**, 489 (1962).

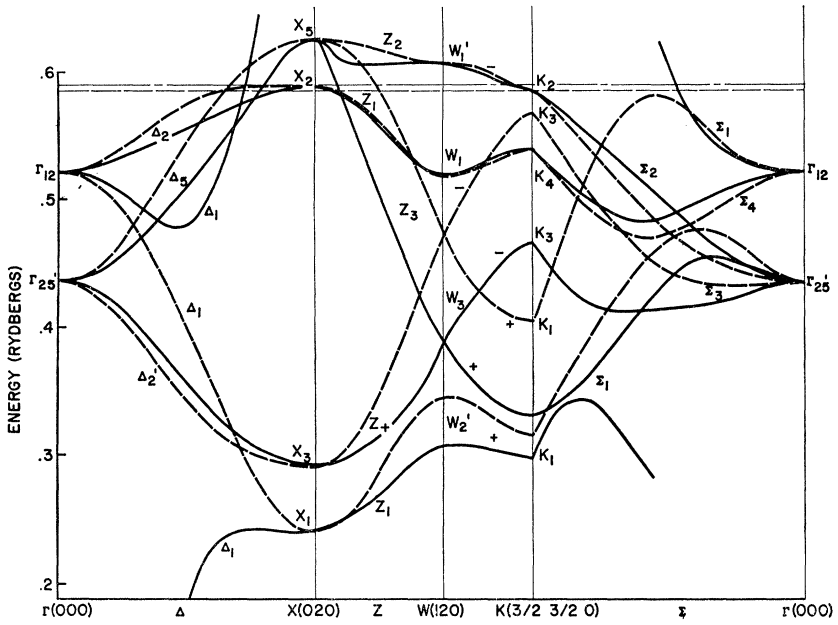

FIG. 1. The energy bands of nickel along symmetry directions. The solid lines are the band structure as calculated by Hanus (Ref. 7) and the dashed lines are the interpolated band structure. The light, constant energy lines represent the two chemical potentials used in the spin-wave dispersion calculation.

by Hanus, are shown in Figs. 1 and 2.[17] The over-all bandwidth, $X_5-X_1=0.386$ Ry, and the splitting, $\Gamma_{12}-\Gamma_{25}'=0.087$ Ry, have been interpolated to agree exactly with Hanus's corresponding quantities, and relatively more attention has been given to fitting the more important higher-lying energies in the d band. As a general observation, for symmetries which do not allow admixing between $3d$ and either $4s$ or $4p$ bands, the interpolated values agree with the calculated values to within 0.02 Ry or around 5% of the bandwidth. On the other hand, where admixing is allowed, the agreement is worsened considerably—to as large as 0.14 Ry. Excluded from these general observations are the symmetry states Δ_1, Σ_1 and Λ_1, in which the d band is overlapped and admixed simultaneously with the $4s$-$4p$ band, causing large splittings of the energy levels.

There are some exceptional states where the fitting is relatively poor, namely, L_1, W_3, K_3 (or U_3). These states admix with the $4s$ band states in the first instance while the latter states admix with $4p$ band states. While the poor fits at W_3 and K_3 might be attributed to such admixture, it is rather unlikely from numerical considerations that the lack of fit at L_1 could be entirely due to admixture. Because of the positions of the energies L_1, W_3, and K_3 in the band, however, such a poor fit should have a minor effect only on the calculated spin-wave spectrum.

Deviations from Hanus' calculated energies about X_5 are observed for Δ_5, Z_3, and S_3, the latter two devia-

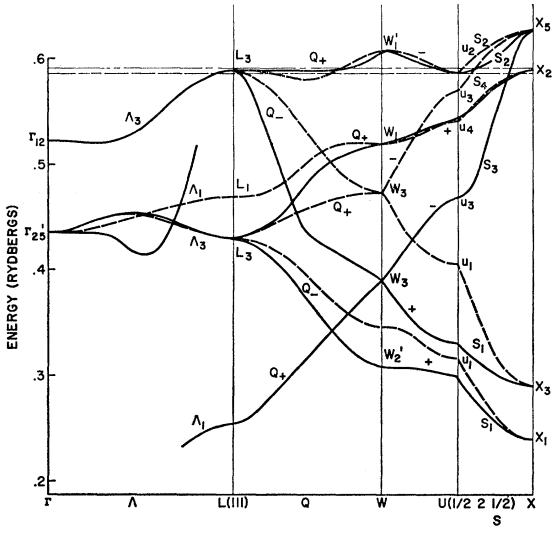

FIG. 2. The energy bands of nickel along symmetry directions. The solid lines are the band structure as calculated by Hanus (Ref. 7) and the dashed lines are the interpolated band structure. The light, constant energy lines represent the two chemical potentials used in the spin-wave dispersion calculation.

[17] A table of interpolated and Hanus's calculated energies at symmetry points is available from the author upon request.

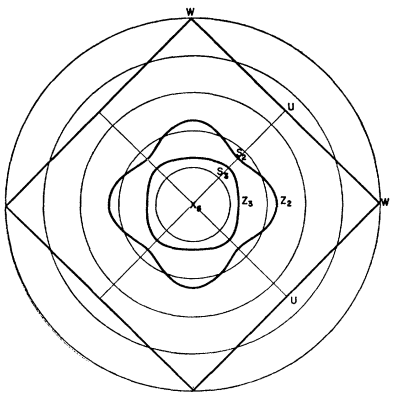

FIG. 3. The constant energy contours of nickel on the square face of the Brillouin zone as calculated by the analytic expansion about X_5 [Eq. (3)]. An effective-mass model for nickel is quite clearly unjustified.

TABLE I. Curvature of the interpolated energy bands near X_5 along different directions, the curvature being expressed in terms of a reciprocal mass normalized to the reciprocal free-electron mass.

Symmetry	Curvature
Δ_5	−0.36
Z_2	−0.22
S_2	−0.388
Z_3	−0.755
S_3	−0.587

tions affecting only the calculated spin-wave mass from the second band. These deviations most likely arise from admixture with $4p$ band states of the same symmetry. No admixture is possible for Z_2 and S_2, however, and the deviations here indicate that Hamiltonian parameters between d-atomic-like states on farther than second-nearest neighbors are required.

The significant energies which concern the spin-wave spectrum are those lying higher than the chemical potential; these are shown as horizontal lines on Figs. 1 and 2. These states have wave vectors lying close to X_5 and the six equivalent square faces of the Brillouin zone. The uppermost band is labeled by the symmetries X_5, Δ_5, Z_2, W_1', and S_2, and the second uppermost band is labeled by X_5, Δ_5, Z_3, and S_3. Expanding the Hamiltonian matrix about X_5, the corresponding eigenvalues are found to be given by the expression

$$E(k_\perp,k_{||},\theta)-X_5=-0.324(k_\perp/k_0)^2 -(k_{||}/k_0)^2[0.439\pm0.182(1+0.757\cos4\theta)^{1/2}]\,\mathrm{Ry}, \quad (3)$$

where $k_0=2\pi/a$, $k_\perp$ is the magnitude of the $\mathbf{k}$ vector perpendicular to the square face as measured from X_5, $k_{||}$ is the magnitude of the $\mathbf{k}$ vector in the square face, and θ is the angle between $k_{||}$ and the line XW.

From this expression, the constant-energy contours in the square face can be calculated, and are as shown in Fig. 3. Particularly for the uppermost band, an effective-mass approximation appears unjustified. Figure 4 shows the actual interpolated energies as well as the energy as calculated from Eq. (3). Equation (3) is a very good approximation for energies above the chemical potential, except for Z_2, where (3) is good for only $\frac{1}{4}$ of the distance XW.

While an effective-mass approximation is not valid, the energy-momentum curvature can be found along different directions from X, and this curvature is related to a reciprocal mass in the usual manner. Results of such curvature study are shown in Table I. The curvature is observed to be an order of magnitude larger than that quoted erroneously[18] from specific-heat results. We shall later compare these curvature results with the effective spin-wave mass.

[18] It has been pointed out previously that the commonly accepted mass of $28m_0$ for nickel based upon specific-heat results is erroneous and too large from the purely geometrical considerations of the multiple band extrema [E. D. Thompson, Bull. Am. Phys. Soc. **9**, 559 (1964)]. The mass found here is even smaller than these geometrical considerations indicated.

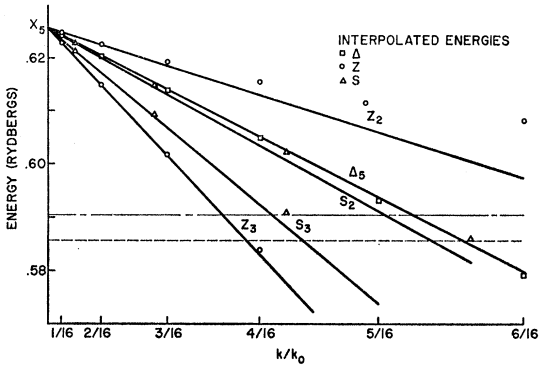

FIG. 4. The energy bands of nickel near X_5 as a function of wave vector measured from X_5. The abscissa is a quadratic scale in momentum. The small circles display the interpolated energies and the solid straight lines display the energy as calculated by the analytic expansion about X_5 [Eq. (3)]. The relevant constancy of the energy band curvature along a fixed direction is observed. The light, constant energy lines represent the two chemical potentials used in the spin-wave dispersion calculation.

C. Density of States

Using the interpolated energy eigenvalues, a density-of-states histogram can be calculated by dividing the energy scale into uniform segments ΔE, counting the number of energy eigenvalues in each segment, and multiplying by the appropriate scaling factor. The resultant density-of-states histogram for two particular energy widths, $\Delta E=0.00917$ and 0.00306 Ry, is shown in Fig. 5. The larger of these two energy widths is only somewhat smaller than that shown by Burdick[19] for the copper "d hump," but we have here 8 times as many eigenvalues due to a smaller k mesh.

A considerable amount of structure can be seen on these histograms, some of which reflect real structure in the density of states. The remaining structure results from the discreteness of numerical calculations. To obtain some idea of the magnitude expected from the latter, an energy eigenvalue occurring at general k contributes 0.32 states/atom Ry for $\Delta E=0.00917$ and 0.96 states/atom Ry for $\Delta E=0.00306$; energy eigenvalues at symmetry k contribute less. Structure less than two or three times this amount cannot be attributed definitely to real structure in the density-of-states function.

Comparing the density of states for nickel and copper,[19] the two are observed to be very similar, but with the copper density of states narrower in energy and larger in magnitude. This occurs even though the copper calculation contains admixture of the d, s, and p bands. General features of the nickel density of states are two large peaks near the top of the band separated by about 0.12 Ry, a somewhat smaller peak between, and a relatively slow decrease of the density of states at the bottom of the band compared to the rapid rise at the top of the band. One feature that differs from

[19] G. A. Burdick, Phys. Rev. **129**, 138 (1963).

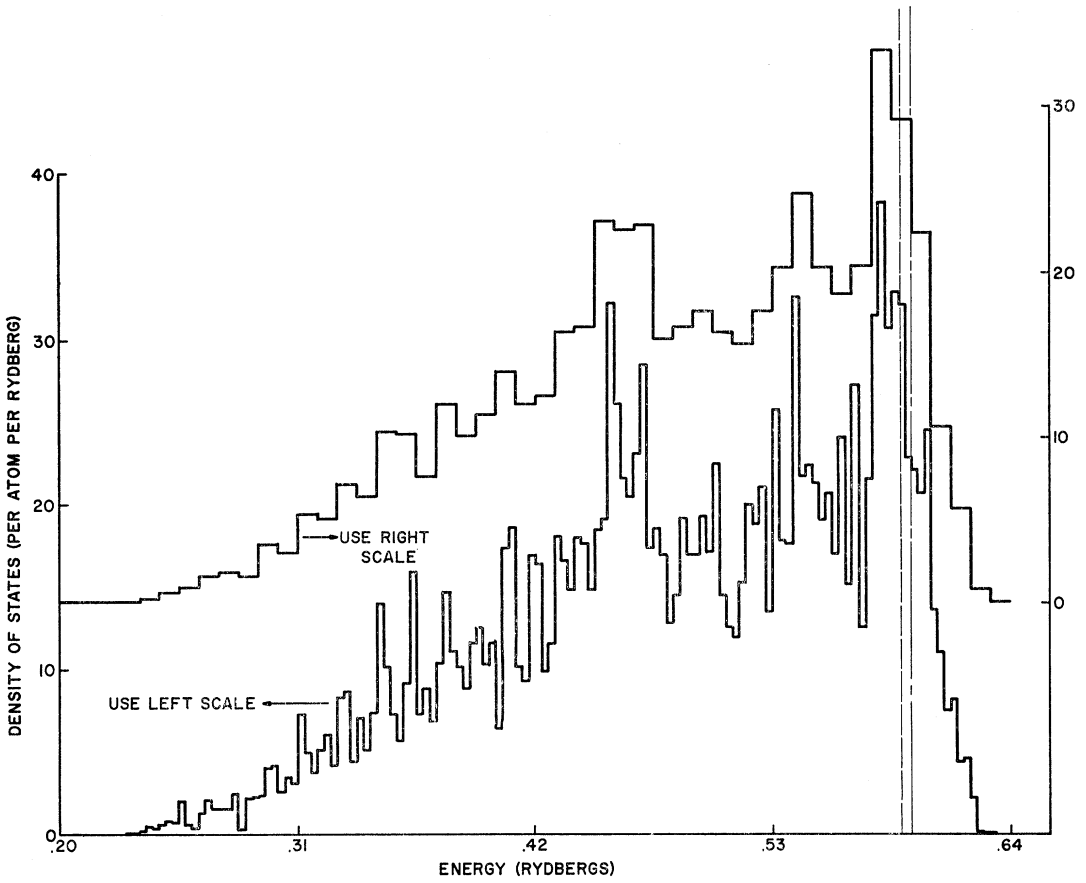

FIG. 5. The density-of-states histogram for nickel as calculated from the interpolated bands. The histogram bar width is 0.00917 Ry for the upper curve and 0.00306 Ry for the lower. The light, constant energy lines represent the two chemical potentials used in the spin-wave dispersion calculation.

copper is that the larger of the two peaks occurs at the higher energy for nickel, the lower energy for copper.

The calculated electronic specific-heat coefficient γ in the specific-heat expression $C_v=\gamma T$ is shown in Table II to be about 25% smaller than the experimental value[20] of 17.4×10^{-4} cal/mole deg^2.

III. SPIN-WAVE DISPERSION

A. Spin-Wave Reciprocal Mass

In combining the interpolated energy bands and the spin-wave dispersion relation Eq. (1), we shall consider the magnetic carriers as holes, the energy of which must be the negative of the corresponding electronic state. Furthermore, we order and label the energy bands as follows. For a fixed $\mathbf{k}$, the largest electronic energy is in the first hole band, the next largest the second hole band, etc. Deferring to Sec. III D consideration of multiple bands, we shall carry out the solution of Eq. (1) using the hole energies from the first hole band.

TABLE II. Electronic-specific-heat coefficient γ in mcal/mole deg^2 for nickel as calculated from the density-of-states function (Fig. 5).

Chemical potential (Ry)	$\Delta E=0.00917$ (Ry)	$\Delta E=0.00306$ (Ry)
0.5905	1.21	0.945
0.5857	1.21	1.324
Peak-of-density function	1.38	1.58

Setting the interatomic exchange integral equal to zero in Eq. (1), the energy of a spin wave with wave vector $[k_0/16,0,0]$ is calculated as a function of the band splitting ΔE_d. From preliminary calculations, it is known that the effective-mass approximation of Eq. (3) is valid for a wave vector of this magnitude and we accordingly express these results, as shown in Fig. 6, in terms of the spin-wave mass normalized to that of a free electron. The band splitting has been normalized to the chemical potential μ' as measured from the top of the band, $X_5-\mu=\mu'$.

Three observations should be noted from the figure. First, the reciprocal mass for infinite band splitting is smaller than the reciprocal mass of the carriers at X_5

[20] W. H. Keesom and C. W. Clark, Physica 2, 513 (1935).

(Table I and Fig. 4). This fact might have been anticipated, because Fig. 4 shows the magnitude of the curvature decreasing as k moves away from X_5 towards W. Second, the reciprocal mass can be analytically fitted to the equations

$$(m_0/m_{sw})=0.175[1-0.706\mu'/\Delta E_d] \quad \text{for} \quad \mu=0.5857,$$
$$(m_0/m_{sw})=0.192[1-0.667\mu'/\Delta E_d] \quad \text{for} \quad \mu=0.5905,$$
$$\text{for} \quad \mu'/\Delta E_d \leq 1. \quad (4)$$

For comparison, the effective-mass energy-band model yields the equation

$$(1/m_{sw})=(1/m_c)(1-0.8\mu'/\Delta E_d),$$

with m_c the carrier mass.

And third, the experimental mass[12] is obtained for $\mu'/\Delta E_d=0.593$ and 0.702 for $\mu=0.5857$ and 0.5905, respectively. If direct interatomic exchange had been included in the calculation, the splitting would necessarily have been smaller in order to obtain the experimental value of reciprocal spin-wave mass.

B. Spin-Wave Energy versus Wave Vector along the Principal Axis

Using the band splitting ΔE_d necessary in obtaining the experimentally observed spin-wave mass, the dispersion relation (1) is solved along the principal axis directions, [100], [110], and [111], from the center to the surface of the first Brillouin zone. The solutions are as shown in Figs. 7 and 8, Fig. 7 showing the continuum band of excitation energies as well as the spin-wave energies.

Important for the thermodynamics of ferromagnetism is the large energy gap that exists between the maximum spin-wave excitation energy and the continuum band of energies, some 2800°K. The existence of such a gap would indicate that the decrease of the saturation magnetization with increasing temperature arises almost entirely from spin-wave excitations.

The energy gap for $\mu=0.5905$ Ry is 200°K (not shown in a figure); for other band splitting values, the energy gap completely disappears. The magnitude of the minimum continuum band and maximum spin-wave excitation energies indicate, however, that, for the cases investigated, decreasing magnetization with increasing temperature arises from spin-wave excitations and that there will be no thermally excited short-wavelength spin waves even at the Curie point of nickel.

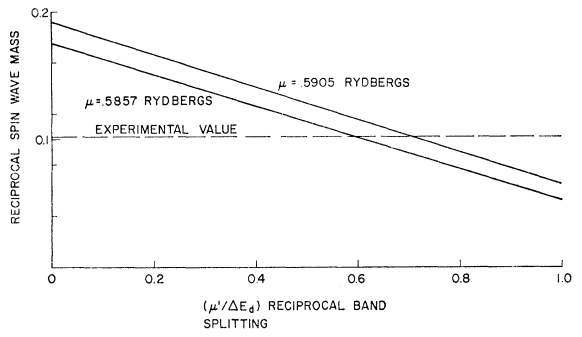

FIG. 6. The dependence of the spin-wave mass on the band splitting. The dashed line indicates the experimental value of the mass for nickel and does not represent any functional dependence on band splitting.

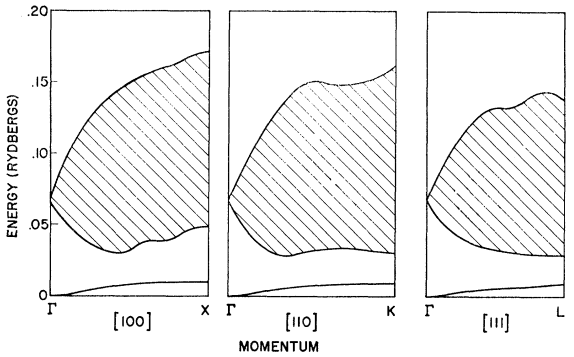

FIG. 7. The momentum dependence of the excitation energy for a single spin reversal in nickel along the three principal axis directions. The lined regions indicate a continuum band of excitation energies and the single line separated from the continuum and going to zero energy at Γ represents the spin-wave energy. The figure is drawn for the chemical potential $\mu=0.5857$ Ry.

The spin-wave dispersion curve remains distinct from the continuum band in both calculations. In contrast, analytical models have the spin-wave dispersion curve either just becoming degenerate with the bottom of the continuum band or entering the continuum band. It is not known at the present time whether the calculated distinctness of the spin-wave dispersion curve is a general result, arising from the Brillouin-zone boundary effects (umklapp), or is a numerical accident.

The maximum energy of a spin wave, which can be expressed as an equivalent temperature θ, is an order of magnitude lower than that usually associated with spin waves. θ values obtained are 1510 and 2100°K for $\mu=0.5857$ and 0.5905 Ry, respectively, and the approximation $T \ll \theta$ made in thermodynamic calculations is no longer valid over the whole temperature range up to the Curie point. Under such circumstances, the finiteness of the number of spin-wave modes must be taken into account.

C. Analytical Fitting

The form of the spin-wave dispersion curves indicates that any power series expansion about $q=0$ would be a slowly converging series, not of practical utility. Moreover, the reciprocal lattice translation properties of $E(\mathbf{q})$ suggest the Fourier series of the form

$$E(\mathbf{q})=\sum_{\mathbf{R}} E(\mathbf{R}) \exp(i\mathbf{q}\cdot\mathbf{R}). \quad (5)$$

In (5), the sum is over all real lattice vectors $\mathbf{R}$ of fcc nickel and the rotational symmetry of $E(\mathbf{q})$ requires

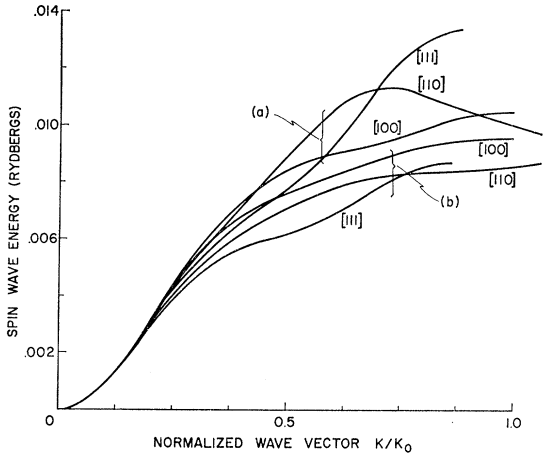

FIG. 8. The momentum dependence of the spin-wave energy in nickel along the three principal axis directions. Curves (a) and curves (b) show the calculational results for the chemical potential $\mu=0.5905$ and 0.5857 Ry, respectively.

$E(\mathbf{R})=E(\mathbf{R}')$ if $\mathbf{R}$ can be rotated into $\mathbf{R}'$ by one of the rotational symmetry elements of the space group.

The number of Fourier terms indicated by Fig. 8 and the limited data available along three spatial directions preclude the evaluation of the three-dimensional transform (5). Let us therefore evaluate a one-dimensional transform independently along the [100] and [111] directions, obtaining from these one-dimensional transforms some idea of the range of $E(\mathbf{R})$.

For $\mathbf{q}=[q,0,0]$, the appropriate series is

$$E(q)=\sum_{n=0}^{\infty} E_n \cos(nqa/2), \tag{6}$$

where a is the edge length of the unit cell. For $\mathbf{q}=[q,q,q]/\sqrt{3}$, the appropriate series is

$$E(q)=\sum_{n=0}^{\infty} F_n \cos(nqa/\sqrt{3}). \tag{7}$$

The relationship between the E_n and F_n of (6) and (7) and the $E(\mathbf{R})$ of (5) is

$$E_n=[2-\delta_{n,0}]\sum_{n_1 n_2=-\infty}^{\infty} E[\tfrac{1}{2}na\hat{\imath}+(n+n_2-n_3)\tfrac{1}{2}a\hat{\jmath}+(n_2+n_3)\tfrac{1}{2}a\hat{k}],$$

and

$$F_n=[2-\delta_{n,0}]\sum_{n_1,n_2=-\infty}^{\infty} E[(n-n_2)\tfrac{1}{2}a\hat{\imath}+(n_1+n_2)\tfrac{1}{2}a\hat{\jmath}+(n-n_1)\tfrac{1}{2}a\hat{k}]. \tag{8}$$

The Fourier coefficients E_n and F_n of (6) and (7) are given in Table III for $\mu=0.5857$ Ry, and the resultant fit to the numerically calculated spin-wave dispersion curve is displayed visually in Figs. 9 and 10. The fit is poor for a two-term series, is qualitatively good for a four-term series, and is quantitatively good for a six-term series. This corresponds, respectively, to $E(\mathbf{R})$ being zero when $\mathbf{R}$ is equal to or greater than that of second-nearest neighbors, eighth-nearest neighbors, and twenty-first-nearest neighbors.

TABLE III. Fourier coefficients E_n and F_n of the nth harmonic of the spin-wave energy along given directions (in Rydbergs).

n/Direction	E_n[100]	F_n[111]
0	6.413, −03	5.144, −03
1	−4.097, −03	−3.625, −03
2	−1.417, −03	−7.391, −04
3	−7.072, −04	−7.284, −04
4	−2.153, −04	−5.171, −05
5	3.691, −06	6.309, −06
6	9.134, −06	3.283, −06
7	1.342, −05	−1.406, −05
8	−3.350, −06	3.944, −06

A power series about $q=0$ gives a poor representation to the spin-wave dispersion curves, as shown in Fig. 8. If we desire a representation which is valid for small q, the appropriate power series is

$$E(\mathbf{q})=A(q/k_0)^2-B(q/k_0)^4+\cdots, \tag{9}$$

with $A=0.0927$ Ry and $B=0.593$ Ry for $\mu=0.5857$ Ry. This representation is found to be valid for $(q/k_0)\lesssim 0.2$.

The coefficients A and B in Eq. (9) are important experimentally[21] in that the coefficients in the magnetization law,

$$\Delta M_n=(M(0)-M(T))/M(0)=CT^{3/2}+DT^{5/2}+\cdots, \tag{10}$$

are given by the relation

$$D/C=8.05[N^{2/3}B/Ak_0^2]C^{2/3}, \tag{11}$$

with N being the number of one-directed spins per unit of volume. We find the dimensionless square bracket on the right side of (11) to be 0.290. This compares favorably with the experimental value of 0.661.[8]

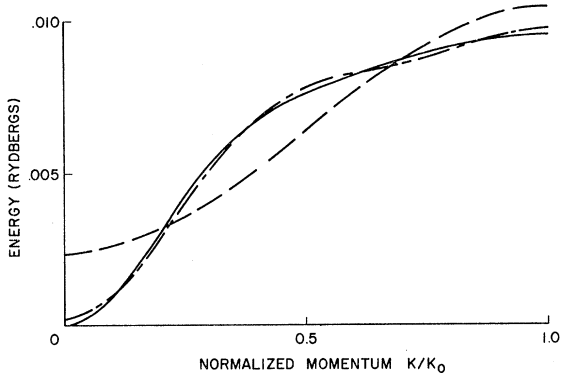

FIG. 9. Fourier fitting of the spin-wave energy along the [100] direction. The dashed curve is drawn for the two-term series, the dot-dash curve for the four-term series, and the solid curve for the six-term series and the calculated curve of Fig. 8, curves (b).

[21] E. D. Thompson, Bull. Am. Phys. Soc. **10**, 16 (1965).

TABLE IV. Summary results.

Chemical potential (Ry)	0.5857	0.5905
Chemical potential μ' (Ry)	0.0397	0.0349
Carriers per atom, 1st band	0.501	0.366
Carriers per atom, 2nd band	0.096	0.077
Reciprocal spin-wave mass m_0/m_{sw}		
1st band, infinite band splitting	0.175	0.192
2nd band, infinite band splitting	0.470	0.475
Experimental value	0.102	0.102
Required band splitting for experimental mass in 1st band (Ry)	0.067	0.0497
μ'/band splitting	0.593	0.702
2nd band normalized reciprocal spin-wave mass for the above splitting	0.262	0.224
Minimum excitation energy to continuum band (°K)	4300	2335
Maximum spin-wave excitation energy along symmetry directions [100], [110], [111] (°K)	1510	2100

D. Multiple Bands

The spin-wave dispersion curve for the case of magnetic carriers contained in more than one band is given as the solution of coupled integral equations, a calculation beyond the initial dispersion calculation presented here. Some idea of the effect of multiple bands upon the dispersion curve can be obtained, however, by considering the long-wavelength limit of the dispersion curve in the absence of interatomic exchange. Under these conditions,[2] a spin-wave mass is defined, m_{sw}, and it is related to the spin-wave mass, m_{swi}, calculated as if the ith band alone were responsible for the magnetic carriers, by the equation

$$(m_{sw})^{-1}=\sum_i N_i(m_{swi})^{-1}/\sum_j N_j. \quad (12)$$

N_i is the number of carriers contained in the ith band, and the summations run over the bands containing magnetic carriers.

Assuming arbitrarily equal splitting for the first and second hole bands, the reciprocal spin-wave mass from the second band is found to be (2.2—2.6) multiplied by the corresponding quantity from the first band. Carrying out Eq. (12), $(m_{sw})^{-1}$ is found to equal 0.128 and 0.123 reciprocal electron masses for $\mu=0.5857$ and 0.5905 Ry, respectively, an increase of some 25% from the experimental value.

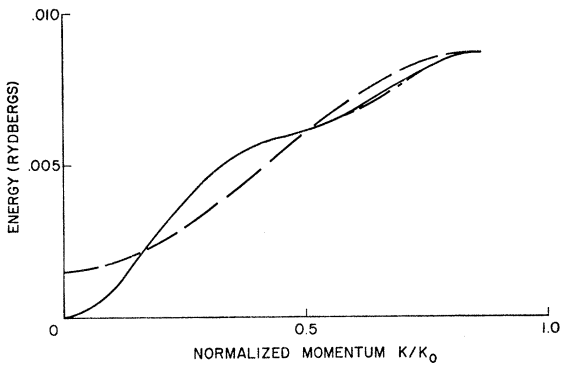

FIG. 10. Fourier fitting of the spin-wave energy along the [111] direction. The dashed curve is drawn for the two-term series, the dot-dash curve for the four-term series, and the solid curve for the six-term series and the calculated curve of Fig. 8, curves (b).

IV. MAGNETIZATION TEMPERATURE DEPENDENCE

The normalized magnetization deviation ΔM_n is defined by the relation

$$\Delta M_n=[M(0°\text{K})-M(T)]/M(0°\text{K}), \quad (13)$$

and is believed generally to result from spin-wave excitations and excitations into the continuum band. To further complicate matters, interaction effects make the continuum and spin-wave bands temperature-dependent in an as yet largely unknown manner. It is worthwhile, however, to calculate ΔM_n neglecting interaction effects and excitations into the continuum band, i.e., the noninteracting spin-wave contribution to ΔM_n. Such a calculation represents a lower bound for ΔM_n.

The neglect of excitations into the continuum band is a good approximation in view of the large energy gap (see Fig. 7 and Table IV) that has been found for such excitations. For instance, using the smaller energy gap of 2335°K, continuum-band excitations contribute 0.003 to ΔM_n at 500°K, or less than 1% of the corresponding contribution from spin-wave excitations. The neglect of interaction effects is a good approximation at temperatures not too close to the Curie temperature; otherwise, it is poor. The exact temperature at which the approximation breaks down is unknown.

Using these approximations,[22]

$$\Delta M_n=[2/N(2\pi)^3]\int_{BZ} d\mathbf{q}[\exp(E(\mathbf{q})/KT)-1]^{-1}, \quad (14)$$

where the integral is carried out over the volume of the Brillouin zone. We have found, as seen in Fig. 8, that the anisotropy in the spin-wave energy is small; i.e., for fixed q, the difference between the maximum and minimum spin-wave energy is small compared to the mean energy. Accordingly, it is a reasonable approximation to define an average energy $\bar{E}(q)$ and to replace the Brillouin zone of (14) by a sphere of equal volume.

[22] E. D. Thompson, E. P. Wohlfarth, and A. C. Bryan, Proc. Phys. Soc. (London) 83, 59 (1964).

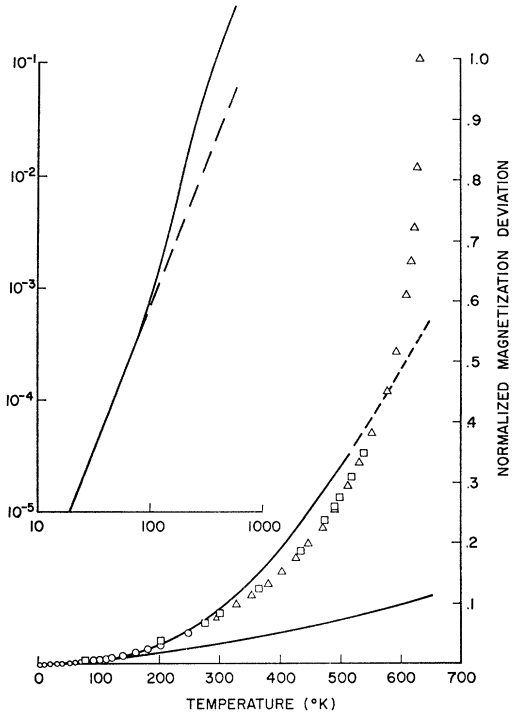

FIG. 11. The normalized magnetization deviation as a function of temperature. Experimental data are as follows: △—P. Weiss and R. Forrer, Ann. Phys. (Paris) **5**, 153 (1926); □—R. L. Streever and L. H. Bennett, Phys. Rev. **131**, 2000 (1963); ○—from Ref. 8. (The higher temperature data are those of Budnick, which are tabulated in Ref. 8.) The uppermost solid curve with dashed high-temperature extension is calculated on the basis of noninteracting spin waves only, the spin-wave spectrum being given in Fig. 8, curves (b). The lower solid curve is the low-temperature $T^{3/2}$ law. The inset log-log plot, showing the difference between the two solid curves as a function of temperature, indicates that the $T^{5/2}$ term in the magnetization law is good to approximately 80°K and that the coefficient agrees with the experimental value of Pugh and Argyle (Ref. 8). The high-temperature results are shown dashed in the main figure, because interaction effects may not be neglected in this region.

Defining $\bar{E}(q)$ somewhat arbitrarily by the average,

$$\bar{E}(q)=0.4E(q,0,0)+0.6E(q/\sqrt{3},q/\sqrt{3},q/\sqrt{3}), \quad (15)$$

an average which has the particular property that the fourth-order anisotropic-momentum term vanishes, the approximate spherical integral to (14) is carried out for the spin-wave band of Fig. 8, curves (b). The results are shown in Fig. 11.

Several features of Fig. 11 worth pointing out are as follows:

(i) Corrections to the low temperature $T^{3/2}$ law equal the $T^{3/2}$ term at 250°K;

(ii) The $T^{5/2}$ correction to the low temperature $T^{3/2}$ law is valid only for temperatures less than 80°K;

(iii) The magnetization deviation calculated is larger than the experimental value for temperatures less than, say 550°K;

(iv) Noninteracting spin waves yield a magnetization deviation of 0.54 at the Curie point.

V. SUMMARY AND DISCUSSION

The spin-wave energy in nickel as a function of wave vector along the three principal directions from the center of the zone to the zone boundary has been calculated on the basis of the theoretical energy bands of Hanus and the assumption of no interatomic exchange. The results of this calculation are summarized in Table IV.

The calculation seems to indicate that single-particle spin-flip excitations will not be thermally excited at temperatures well below the Curie point because of the relatively large energy gap that has been found for such excitations. However, the energy gap will decrease if some interatomic exchange is assumed, and the calculation cannot be conclusive on this point. Moreover, the rather cursory investigation of multiple band effects indicates also a somewhat smaller gap than that contained in Table IV. The energy gap for single-particle excitations is very sensitive to the assumed parameters.

The calculation supports the previous suggestion[21] that the large q^4 term in the spin-wave dispersion results from the detailed shape of the one-electron spectrum rather than from any long range interatomic exchange. The $T^{5/2}$ term in the magnetization law, predicated upon the q^4 term, is only somewhat less than that found experimentally.[8] This fact, coupled with the large energy gap found for single-particle excitations, favors a spin-wave interpretation of the magnetization temperature dependence at low temperatures rather than a combined spin-wave–single-particle interpretation.[22]

We have found that, on the basis of our calculated dispersion relation, the calculated magnetization deviation increases faster with temperature than does the experimental result. This indicates that the energies calculated for short-wavelength spin waves are too small. Using this, the spin-wave spectrum of Fig. 8, curves (a), based upon fewer holes in the d band, would give a calculated magnetization deviation more in agreement with experimental results than that of Fig. 8, curves (b).

For the calculations performed as described in the text, we have found no indication of a cutoff momentum or a $q_{\max}$. The spin-wave spectrum always remained distinct from the continuum band of single-particle excitations. In this connection, it should be pointed out again that the conduction band is assumed explicitly to be noninteracting with the d bands. Obviating this assumption, it is felt that a cutoff momentum would be found.

APPENDIX A: SLATER-KOSTER INTERPOLATION

The Slater-Koster Interpolation[10] is based upon the tight-binding approximation to energy bands in which Bloch waves $\psi_n(\mathbf{k})$ of wave vector $\mathbf{k}$ are constructed as a linear combination of atomic waves $\phi_j(\mathbf{k})$, with

$$\phi_j(\mathbf{k})=N_a^{-1/2}\sum_{\mathbf{R}}\exp(i\mathbf{k}\cdot\mathbf{R})a_j(\mathbf{R}), \quad (A1)$$

where $a_j(\mathbf{R})$ is an atomic function of the jth type at the $\mathbf{R}$th site. The atomic functions are assumed to form an orthonormal set. The coefficients c_{nj} of the linear combination

$$\psi_n(\mathbf{k})=\sum_j c_{nj}(\mathbf{k})\phi_j(\mathbf{k}) \tag{A2}$$

are determined by the variation principle, and the one-electron energies $\epsilon_n(\mathbf{k})$ are obtained as solutions of the determinantal equation

$$\mathrm{Det}\{\langle\phi_m|H|\phi_j\rangle-\delta_{mj}\epsilon_n(\mathbf{k})\}=0, \tag{A3}$$

where H is the Hamiltonian operator. In view of (A1), the Hamiltonian matrix elements of (A3) can be expressed as products of the matrix elements;

$$\langle m|H|j(\mathbf{R})\rangle=\langle a_m(\mathbf{0})|H|a_j(\mathbf{R})\rangle, \tag{A4}$$

and sines and cosines of argument $\mathbf{k}\cdot\mathbf{R}$. The interpolation scheme treats the matrix elements of (A4) as disposable parameters, determined so that the solutions of (A3) fit exactly the energies calculated by other techniques at discrete points in $\mathbf{k}$ space for band index n.

TABLE V. Atomic functions.

Label m	Formula
1	$xyR_1(r)$
2	$yzR_1(r)$
3	$zxR_1(r)$
4	$(x^2-y^2)R_2(r)$
5	$3^{-1/2}(3z^2-r^2)R_2(r)$

This procedure is applied here, using matrix elements (A4) between $3d$ atomic functions only. Thus, the determinant of (A3) is of order 5×5, and the roots for a given $\mathbf{k}$ are labeled in descending order: Band 1 is the highest root; band 2 the second highest; etc. The $3d$ functions appropriate to the cubic symmetry of nickel are used and are labeled as given in Table V.

Disposable parameters among these five atomic functions are restricted to the zeroth ($\mathbf{R}=\langle000\rangle$), first ($\mathbf{R}=\langle110\rangle$) and second ($\mathbf{R}=\langle200\rangle$) neighboring sites. Taking into account the cubic point-group symmetry and the transformation properties of these atomic functions, the number of disposable interpolation parameters is 12. These 12 parameters are obtained by fitting

TABLE VI. Hamiltonian parameters (Ry).

Element	Value	Element	Value	Element	Value
$\langle1\|H\|1(000)\rangle$	0.4988	$2\langle1\|H\|1(002)\rangle$	0.0100	$2\langle4\|H\|4(200)\rangle$	−0.0088
$4\langle1\|H\|1(110)\rangle$	−0.1315	$\langle4\|H\|4(000)\rangle$	0.4679	$2\langle4\|H\|4(002)\rangle$	−0.0099
$4\langle1\|H\|1(011)\rangle$	0.0360	$4\langle4\|H\|4(110)\rangle$	0.1141	$4\langle1\|H\|2(101)\rangle$	0.0182
$2\langle1\|H\|1(200)\rangle$	−0.0074	$4\langle4\|H\|4(011)\rangle$	−0.0165	$4\langle2\|H\|5(011)\rangle$	−0.0319

Hanus's calculated energies[7] at the following 12 symmetry points[13]: Γ_{12}, Γ_{25}', X_1, X_2, X_3, X_5, W_1, W_1', U_2, U_4, L_3, and L_3.

With the exception of X_1, W_1, and U_4, these symmetry points have the advantage that there is no admixture between the $4s$-$4p$ and $3d$ bands. Moreover, the admixture and the resulting changes in the $\epsilon_n(\mathbf{k})$ at these points is small because of the large energy difference between the pure $4s$-$4p$ bands and the $3d$ bands. Hence, the parameters obtained accurately describe the pure $3d$ bands. The parameters used for the interpolated energy bands are tabulated in Table VI.